Rubin M1M3 Support System Dynamic Performance

Bruno C. Quint[a], Felipe Daruich[b], Petr Kubánek[c], Douglas R. Neill[a], Guillem Megias[d,e], Adrian Shestakov[n], Alysha Shugart[b], Andrea Jeremie[f], Benjamin Levine[a], Brian Stalder[a], Craig Lage[g], David Sanmartim[b], Dominique Boutigny[f], Elana Urbach[h], Erik Dennihy[a], Freddy Muñoz Arancibia[a], Holger Drass[b], HyeYun Park[i], Ignacio Sevilla-Noarbe[j], Ioana Sotuela[b], Jacques Sebag[b], Joaquín Hernández[n], Jeffrey Carlin[a], Karla Aubel[b], Kevin Fanning[l], Kevin Reil[l], Laura Toribio San Cipriano[j], Merlin Fisher-Levine[a], Peter Ferguson[m], Roberto Tighe[b], Sandrine Thomas[a], Tiago Ribeiro[a], and Yijung Kang[l]

[a]Vera C. Rubin Observatory Project Office, Tucson, AZ, USA
[b]Vera C. Rubin Observatory, Avenida Juan Cisternas #1500, La Serena, Chile
[c]Institute of Physics, Academy of Sciences of the Czech Republic, NaSlovance 2, 182 21 Praha 8, Czech Republic
[d]Department of Aeronautics and Astronautics, Stanford University, Stanford, CA, USA
[e]Kavli Institute for Particle Astrophysics and Cosmology, SLAC National Accelerator Laboratory, Stanford University, Stanford, CA 94025, USA
[f]LAPP, Université Savoie Mont Blanc, CNRS/IN2P3, Annecy; France.
[g]Physics Department, University of California, One Shields Avenue, Davis, CA 95616, USA
[h]Department of Physics, Harvard University, 17 Oxford St., Cambridge MA 02138, USA
[i]Duke University, Science Dr, Durham, NC 27710, USA
[j]Centro de Investigaciones Energéticas, Medioambientales y Tecnológicas, Av. Complutense 40, 28040 Madrid, Spain
[l]SLAC National Accelerator Laboratory, 2575 Sand Hill Rd., Menlo Park, CA 94025, USA
[m]Department of Physics, University of Wisconsin-Madison, Madison, WI 53706, USA
[n]Instituto de Astrofísica, Pontificia Universidad Católica de Chile, Casilla 306, Santiago, Chile

ABSTRACT

The Vera C. Rubin Observatory is reaching the final stages of its construction and integration, advancing towards its 10-year Legacy Survey of Space and Time (LSST). One of the key milestones was the installation of the M1M3 Mirror Cell Assembly onto the Simonyi Survey Telescope's (SST) Telescope Mount Assembly (TMA). The Cell Assembly actively supports the primary/tertiary mirror (M1M3), playing a crucial role in maintaining the glass safe and ensuring image quality. However, before the mirror glass installation, the Cell Assembly was installed on the TMA while supporting a steel surrogate M1M3 mirror. This surrogate closely mimics the glass mirror's mass, center of gravity, and geometry. The M1M3 cell and surrogate were tested under conditions that simulate rapid field changes in the sky, which are essential for the observatory's ambitious sky mapping schedule. These tests, extending from 1-100% of designed telescope slew velocities/accelerations, assessed the M1M3 active mirror support system, including the force balance system's performance, the hardpoint behaviors, and the efficacy of the pneumatic figure control actuators. Preliminary results suggest the system meets operational requirements, ensuring safety and effectiveness at full speed.

Keywords: LSST, Rubin Observatory, M1M3, Inertia Compensation, Active Supports

Further author information: (Send correspondence to B.Q.)
B.C: E-mail: bquint@lsst.org, Telephone: +56 51 2205 200

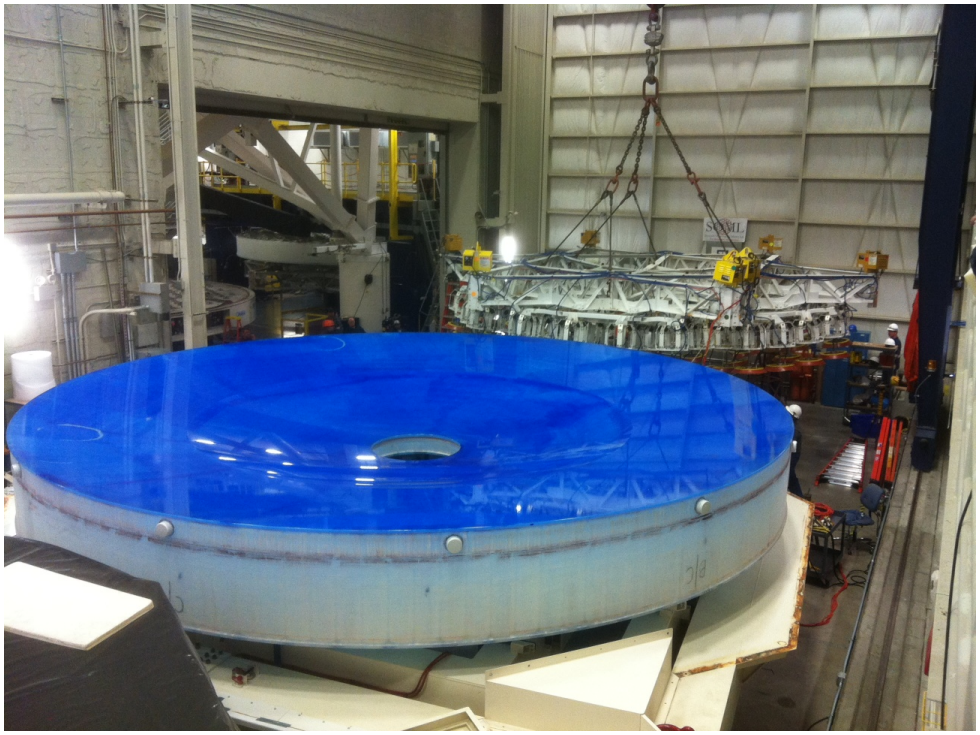

Figure 1. M1M3 glass with a blue protective coat used for storage and transport.

	Velocity (m/s)	Acceleration (m/s^2)	Jerk (m/s^3)
Azimuth	10.5	10.5	42
Elevation	5.75	5.75	21

Table 1. TMA maximum motion settings.

1. INTRODUCTION

The Vera Rubin Observatory, now approaching the final stages of construction, stands as a monumental project poised to revolutionize our understanding of the cosmos through the Legacy Survey of Space and Time (LSST). Tasked with executing this decade-long mission, the observatory aims to address major scientific endeavors: unraveling the mysteries of dark matter and dark energy, cataloging the Solar System's myriad objects, exploring the transient astronomical sky, and mapping the structure and evolution of the Milky Way and beyond. Achieving this goal requires the observatory to rapidly slew across the sky, which introduces significant engineering challenges.

One of these challenges involves a key component, the 17-metric-ton, 8.4-meter primary/tertiary mirror (M1M3) (Figure 1), which is being prepared for installation on the Simonyi Survey Telescope (SST). To fulfill the observatory's objective of completing a sky mapping within just three nights,[1] the telescope mount has been designed to support slews with high velocities and accelerations. SST is expected to perform slews of up to 3.5 degrees most of the time on the sky and settle within 4 seconds.[2] An additional second is set aside for the Active Optics System (AOS) convergence before imaging, leading to a total of 5 seconds between exposures. It is designed to reach a maximum velocity and acceleration of 10.5 deg/s and 10.5 deg/s^2 in Azimuth and 5.25 deg/s and 5.25 deg/s^2 in elevation[3] (See Table 1). These specifications pose a significant engineering challenge, as no 8m class mirror has previously been subjected to such high accelerations and velocities. The rapid slews generate substantial inertial forces on the mirror.

To allow the use of M1M3 on SST in these conditions, the mirror will be installed on the M1M3 Cell,[4,5] which is composed of two main systems: the Mirror Support System (SS) and the Thermal Control System. The SS provides positioning, support, and figure control for the mirror. Its design consists of six axially stiff linear displacement actuators (termed "hardpoints" or HPs)[6,7] and 156 pneumatic figure control force actuators

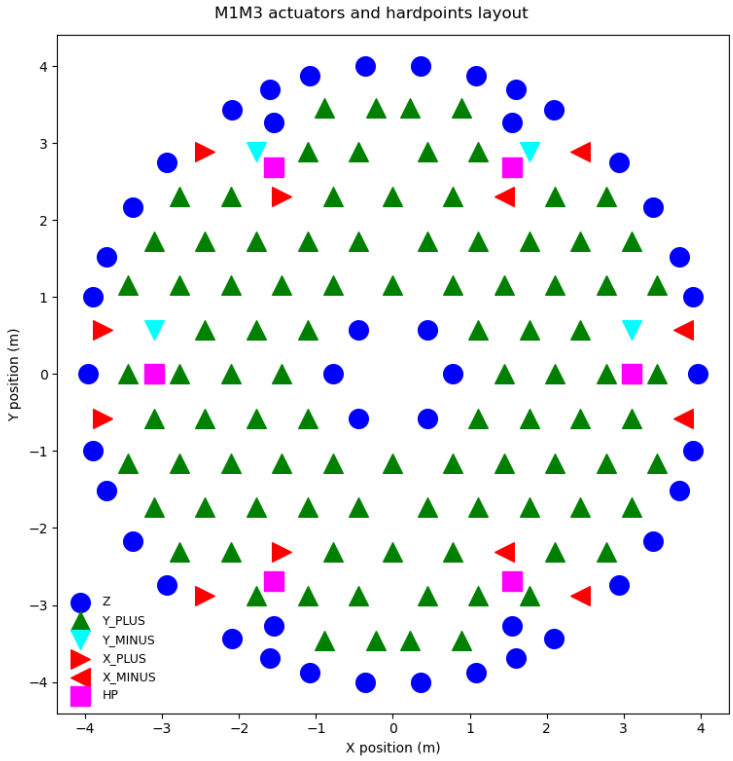

Figure 2. Hardpoints and force actuators approximate position on M1M3. Single-axis force actuators are represented as blue circles. Double-axis force actuators are represented as triangles pointing toward their secondary axis. Hardpoints are marked as pink squares.

(FA). 44 of these force actuators are single-axis and provide support only in the axial direction (parallel to the telescope's optical axis). 100 of them are dual-axis, providing support in the axial and lateral direction. 12 FAs are dual-axis, providing support in the axial and cross-lateral directions. Figure 2 shows the different types of force actuators (single-axis versus double-axis), their approximate position, and their orientation (in the case of double-axis actuators).

The hexapod configuration of the hardpoints provides six degrees of freedom for positioning the mirror with respect to the mirror cell, allowing the mirror to translate and rotate along the three coordinate axes. The hardpoint actuators are designed to only define the position of the mirror with respect to the mirror cell without holding any of the cell's weight. The forces measured on the hardpoints should nominally be kept at zero during normal operations.

The force actuators provide mirror support, optimize the optical figure through interactions with the AOS, and counteract inertia forces. The gravity/elevation forces component is compensated using a look-up table (see Section 3). The figure and shape of the mirror, including manufacturer residual aberration, are corrected using the Force Balance System (FBS), which is a closed-loop system that reads the residual forces on the hardpoints and offloads them onto the FAs. Finally, the inertial forces generated by rapid slews are counteracted by the Inertia Compensation System (ICS) (see Section 2), a subsystem that uses telemetry from DC accelerometers and gyros to calculate acceleration and velocity forces to be applied to the force actuators for minimizing these inertia effects.

Prior to installing the M1M3 glass on its cell and then on SST, it is essential to confirm its safety through testing with a steel surrogate (Figure 3). This surrogate is a mechanical structure used only for tests, and it has mechanical properties similar to those of a glass mirror, such as mass, center of gravity, and geometry.

We successfully mounted the M1M3 steel surrogate and cell onto the SST in late April 2023. The M1M3 cell was fully populated with its mirror support system, including the force actuators and hardpoints. This

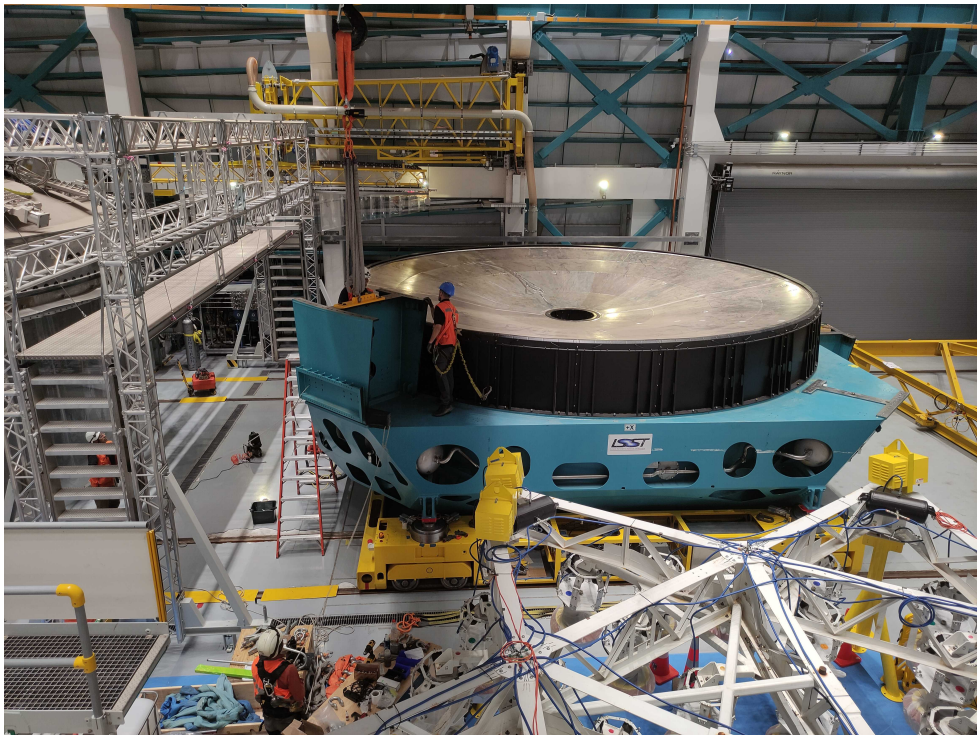

Figure 3. M1M3 Cell with the M1M3 steel surrogate installed on it. Rubin Observatory/NSF/AURA/M. Rivera.

installation was followed by an extensive testing campaign, demonstrating that the M1M3 Cell system will likely meet its operational demands. This includes maintaining safe and efficient mirror functionality even at the telescope's full dynamic capabilities.

We divided these tests into quasi-static and dynamic tests. The quasi-static tests were designed to confirm the system's safety under controlled conditions, operating at no more than 10% of its maximum velocity, acceleration, and jerk. The primary purpose of these tests was to verify that the mirror's support system could effectively counteract the variations in gravitational orientation as a function of elevation angle. These tests evaluated the behavior of the hardpoints, their breakaway system,[8] the performance of the 156 pneumatic figure control actuators,[9] and the efficacy of the M1M3 Force Balance System.[10] The dynamic tests, on the other hand, were integral to the development cycle of the inertia compensation system, involving the telescope operating with a performance ranging from 10% up to its maximum acceleration and velocity.

The outcomes of the quasi-static tests are detailed in Section 3, and those of the dynamic tests in Section 4. For further details on the inertia compensation system, refer to Section 2, which follows.

2. INERTIA COMPENSATION SYSTEM

The M1M3 Mirror Support System (SS) was engineered to mitigate the influence of gravity/elevation and inertial forces. The gravity/elevation forces are calculated as a function of the elevation angle using a modified look-up table (LUT), which contains the coefficients of a 5th-degree polynomial for each force actuator. In contrast, the forces associated with the fast movement of the telescope are computed using the Inertia Compensation System (ICS). This sub-system comprises a set of accelerometers and gyro sensors that measure the telescope's motion when slewing, and it commands additional forces to the FAs to counteract these dynamic loads.[11] The residual forces not compensated by the gravity/elevation forces nor by ICS are compensated using the Force Balance System.

The ICS comes into play when the telescope slews in azimuth, elevation, or both axes. Since the telescope undergoes relatively large slewing accelerations and velocities, excessive load would be produced on the hardpoints. The hardpoints feature a pneumatic breakaway system that enters into play when forces above a certain

limit are applied to them. When a breakaway happens, the hardpoints lose stiffness, and their position becomes unconstrained, thus losing the telescope optical alignment.[11]

For mirror safety and operational efficiency purposes, the hardpoints should not break away during a normal telescope slew. Consequently, the FAs will be used during a slew to counteract the resulting dynamic loads and avoid breaking away. If the system works correctly, the forces measured by the six hardpoints should be negligible.

During a slew, the M1M3 Mirror support system controller computes the inertial forces based on the state of motion of the mirror cell and uses eight force-distribution matrices to account for the eight mirror cell motions (three forces, three moments, and two precession terms). The actual state of motion of the mirror cell is determined using four DC accelerometers and a gyro that provides angular velocity and angular acceleration in the three mirror cell axes. During the slew, these compensatory inertial forces are fed to the actuators at 50 Hz. Although the hardpoints may see additional force loading during slews, these extra forces shall remain below the M1M3 repeated load force limits.

The mirror is safe if the measured forces on the hardpoints are below their breakaway limit. The breakaway limit is set to limit the force to the hardpoints to a quasi-static limit. However, to prevent eventual fatigue failure due to the extremely high cadence of the TMA, we defined two other limits to be monitored during the tests and slews. Our calculations show that, for a borosilicate mirror, the fatigue limit corresponds to approximately 30% of the hardpoints breakaway nominal limit (see the subsection 3.2). To ensure safe system operating conditions over the ten-year survey, we picked a safety factor of 0.5, which is normally used when the exact value for a given material is unknown. This means we decided on a safe operational limit defined as 15% of the nominal breakaway limit.

The actual breakaway limit of each hardpoint was empirically determined through a series of controlled tests that applied incremental compression and tension forces to gauge the triggers of this safety mechanism. These crucial tests form part of the quasi-static testing regime described in Section 3 below. These are key to validating the telescope's support systems and operational safety before advancing to dynamic testing scenarios.

3. QUASI-STATIC TESTS

In late April 2023, the M1M3 cell and its steel surrogate were installed on the TMA. This marked the beginning of a test campaign designed to incrementally assess the telescope's mechanical and operational thresholds. This important phase concluded in February 2024, when the surrogate and its cell were removed from the TMA to replace the surrogate with the M1M3 glass and subsequently be prepared for coating.

The campaign began by thoroughly verifying the safety interlock system and ensuring all safety mechanisms were correctly engaged. After that, we performed a battery of tests that considered the most critical components: the force actuators, the hardpoints, and the elevation/gravity forces.

3.1 Force actuators bump tests

We started quasi-static tests with the so-called "bump tests" to assess the health of each FA before the mirror was raised. These tests involved applying a 222 N force in both push and pull directions. A test was considered successful if the discrepancy between the applied and measured forces was less than 5 N. Figure 4 shows an example of a bump test applied to one of the dual-axis actuators.

Conducted on a daily basis, these tests occasionally identified actuator failures, shifting the focus from simple verification to critical health checks. Actuators failing this test twice necessitated immediate hardware intervention. Only 4 double-axis actuators that failed the bump test were replaced by spare actuators. All of them presented problems with one pressure servo valve, which was replaced, and the actuators were tested and stored as spares.

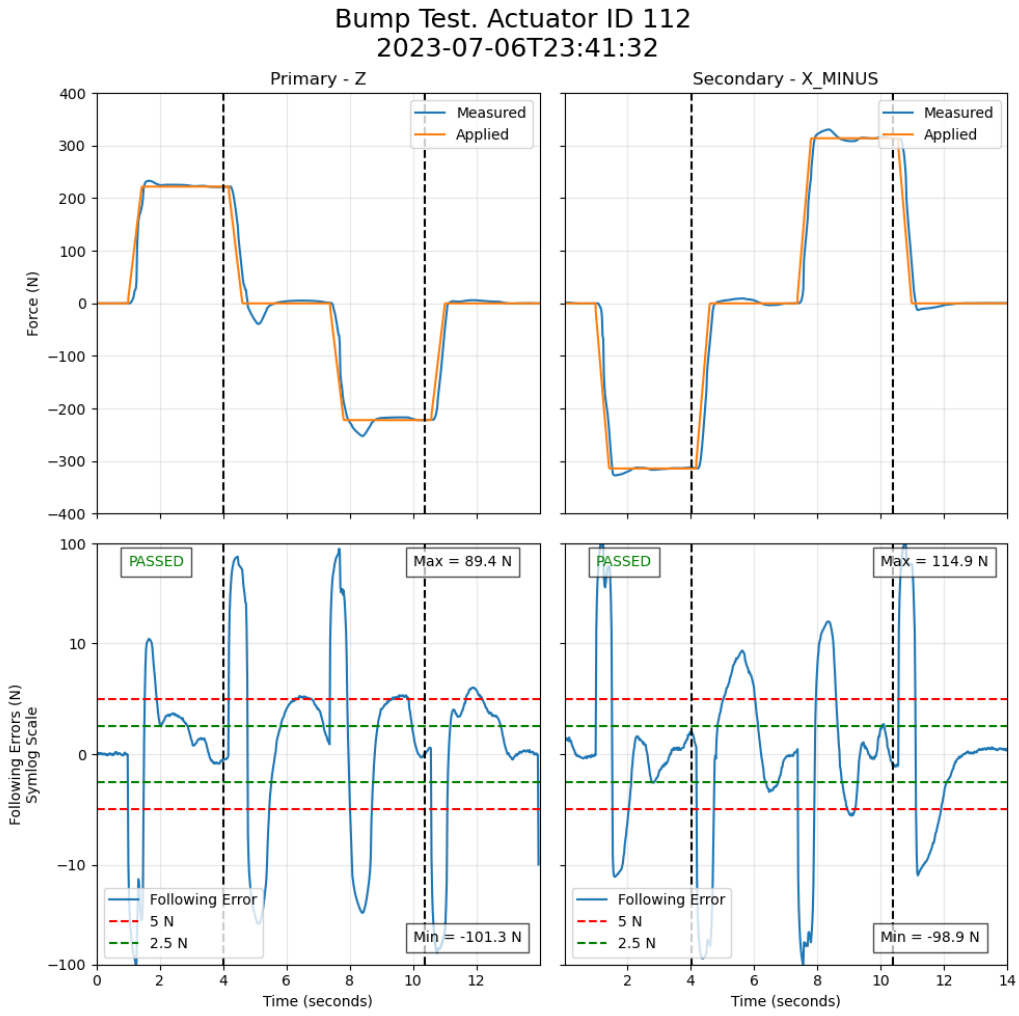

Figure 4. Bump test following errors. The dotted vertical line shows where the pass/fail decision is made, depending on the settling time. The bump test passes if this is within the red lines. In the two lower plots, the y-axis has a symlog scale with a linear scale between ±10 N and a log scale beyond those values.

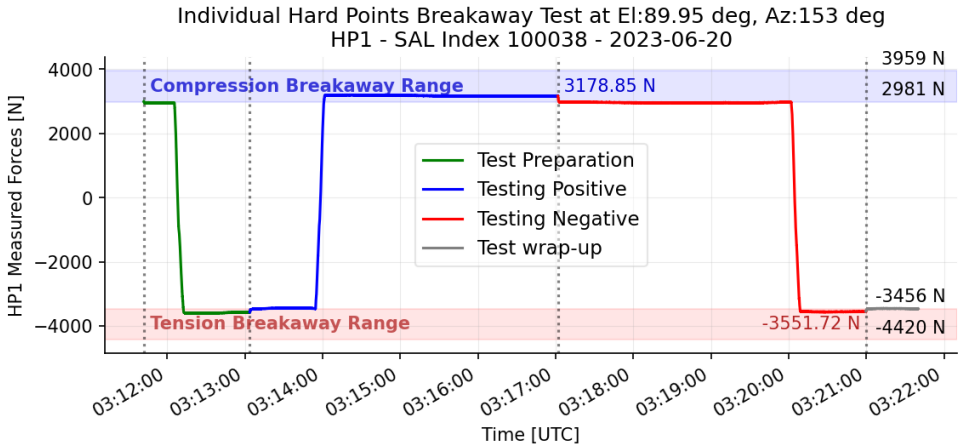

Figure 5. Hardpoint breakaway test example. It shows that the HP1 breakaway point is within the required range when applying an external compression and tension force.

3.2 Hardpoints breakaway tests

The subsequent set of tests validated the hardpoints' breakaway system, which is vital for the safety of the glass. Each hardpoint is designed to disengage under excessive load, with the breakaway system activated by tension forces between -4420 N and -3456 N and compression forces between 2981 N and 3959 N. Analysis of test data confirmed the hardpoints' breakaway limits to be -3600 N $\pm$ 33 N in tension and 3150 N $\pm$ 56 N in compression. The asymmetry in the tension forces versus the compression forces comes from the fact that the pressure inside the breakaway system is the same, but the size of the pistons is different in the two different directions.

Figure 5 shows an example of a hardpoint breakaway test. The light-blue shade and light-red shade strips at the top and at the bottom of the plots show the range in which the breakaway should happen. The blue line shows the response of the hardpoint when an external force towards compression is applied. The breakaway happens, and the force measured on the hardpoint becomes constant at 3178.85 N, which is within the expected range in compression. The same is done in the direction of tension, and we find the breakaway happening at -3551.72 N, which is also within the expected range. Since each hardpoint breakaway has different compression/tension forces, we adopted a uniform breakaway limit of $\pm$ 3000 N in both tension and compression to simplify the analysis while maintaining a conservative approach to system safety.

3.3 Gravity look-up table tests

Subsequent tests expanded to include variable elevation angles while maintaining a constant azimuth position. These adjustments were crucial for balancing the telescope and assessing the system's response to gravitational forces at different angles. The system responds to the variation in elevation angle by varying the forces to the 156 FAs. These forces are calculated by the elevation look-up table (LUT), which contains the coefficients of a 5-degree polynomial fit of the gravity loads versus the elevation angle for each actuator. The LUT, a critical component of the telescope's operational software, contains coefficients that calculate the necessary forces for each actuator to counteract gravitational forces on the mirror and minimize the load on the hardpoints. The initial coefficients were calculated from the mirror's Finite Element Analysis (FEA) model and have been validated.[12]

The fine-tuning of the polynomials involved systematically slewing the telescope from 90 degrees in elevation down to 0 degrees and back up, refining the coefficients by comparing expected to actual forces, thereby ensuring optimal performance. When the FBS is deactivated, the actuators provide forces to counteract gravity based solely on the LUT. These forces should ideally minimize the hardpoint load. Conversely, when the FBS is active, it provides additional corrections based on real-time hardpoint feedback through load cells in the hardpoints, enhancing the system's responsiveness and accuracy. Both the force residuals, measured on hardpoints and distributed to the force actuators or applied FBS forces, can be used to improve the LUT polynomial fit of the mirror response to elevation. Figure 6 shows the forces measured on the hardpoint when the telescope points

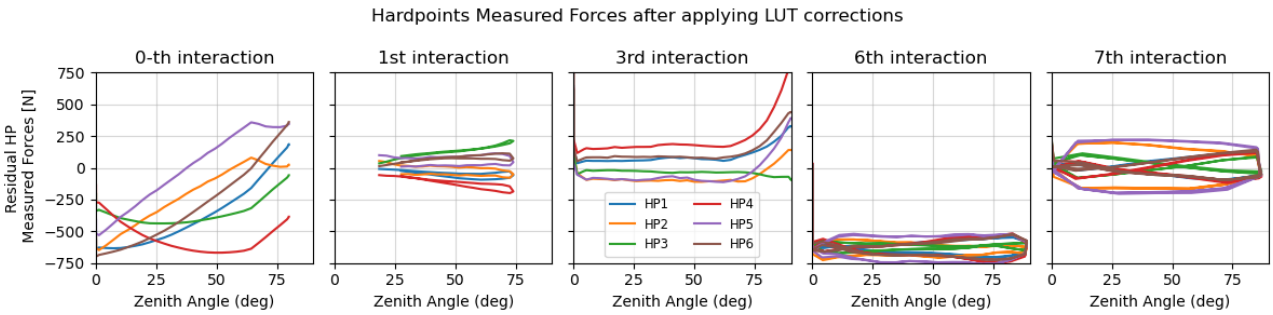

Figure 6. Look-up table evolution shown as different interactions. The first plot on the left shows the initial condition. The forces measured in the hardpoints with the force balance system disabled evolved over different interactions. The last plot on the right shows how the look-up table finally provided corrections that allowed measured forces to assume small values centered at zero.

at different elevation angles and with the inactive FBS. An ideal look-up table brings these forces down to zero or a minimum, partially achieved on the last interaction. However, the system's hysteresis imposed an extra challenge in improving the LUT.

With the telescope freshly assembled, initial movements were executed at 1% of the telescope's maximum operational performance settings for velocity, acceleration, and jerk. Each movement was closely monitored to ensure that the forces on the hardpoints remained well below the breakaway thresholds. As the confidence in the system increased and control loop adjustments were implemented based on real-time data feedback, we incrementally raised the operational intensity. This methodical enhancement continued in 1% increments until reaching 10% of the telescope's maximum capabilities (see Table 1 for the maximum motion settings).

4. DYNAMIC TESTS

Following the initial quasi-static tests, we transitioned to the dynamic testing phase. This phase was crucial for integrating and tuning the Inertia Compensation System (ICS), which had never been fully tested or validated before. We started them by setting the limit of the maximum acceleration, velocity, and jerk to 10% of the values in table 1 and by running two specific tests. The first, called gateway tests, consisted of single-axis movements with long ($> 3.5\,\mathrm{deg}$) and short ($\leq 3.5\,\mathrm{deg}$) slews. These were used to evaluate the system of the M1M3 cell and surrogate, allowed an initial tuning of the ICS, and helped us understand some of the encountered issues (see subsection 4.1).

In addition to these targeted single-axis movements, we performed comprehensive end-to-end performance tests, also called soak tests,[13] using the same performance level once the ICS was tuned enough to have measured forces in the hardpoints below the breakaway limits. These tests, involving scheduler-driven survey simulations with short and long slews in any requested direction, utilized the full Simonyi Telescope and all subsystems: the TMA, the M1M3 surrogate and its cell, the M2 surrogate and its cell, the two hexapods and the rotator. The primary objective was to ensure that all systems could operate seamlessly over extended periods without faults. However, we used the soak tests as a form to evaluate the behavior of M1M3 and the ICS during the survey. The volume of slews performed—typically exceeding 300 per night— enabled a robust statistical analysis of the inertial compensation system's efficacy.

We repeated the gateway and soak tests while incrementing the velocity, acceleration, and jerk limits to 20% and 30% until they reached 100%. See the two subsections below for more details on these tests.

4.1 Gateway tests and initial challenges

As we initiated the dynamic tests, we performed short ($\leq 3.5\,\mathrm{deg}$) and long ($> 3.5\,\mathrm{deg}$) slews in the azimuth and elevation directions. We paid special attention to the azimuth movements since this is the direction that introduces the strongest inertial forces on the mirror. By isolating the movement to this single axis, we analyzed

the effects of the acceleration and velocity components, thereby gaining precise insights into the inertial impacts. This specificity was crucial in effectively tuning the ICS to counteract these forces dynamically.

Nominally, the ICS utilizes accelerometers and a gyroscope, along with telemetry data from the telescope mount, to calculate the necessary counteracting forces in real-time. However, at the beginning of this test campaign, we discovered that the DC accelerometers' axes were not properly aligned with the movement axes, and the gyroscope did not provide the required data.

We attempted to use the telemetry from the telescope mount alone, but the latency in the data stream was too large ($> 150ms$) to work properly. After many iterations, we got the accelerometers' axes properly aligned. After aligning the DC accelerometers' axes, we learned that the signal processing of the accelerometers' signal needed improvements. Instead of using a single measurement during the control loop, we took as many measurements as feasible, let the Field Programmable Gate Arrays (FPGAs) calculate the rolling median, and report that as the final value during the 20ms loop. This approach significantly increased the signal-to-noise ratio, allowing us to use the DC accelerometers' signal as initially intended. Instead of using the gyroscope data to calculate and correct the velocity forces, we let the FBS do the work during slews. In other words, the FBS was enabled both when slewing and tracking, and the ICS would be enabled only for the duration of the slew.

In addition to the improvements above, we successfully experimented with different PID (proportional-differential-integral) control loop settings in the FBS. This allowed the mirror to reduce the time the system needs to react to errors (mostly increasing the P term of the PID). This led to discontinuity of the FBS force values, as the system needed some time to adjust its response. That was trivially fixed by freezing the FBS forces from non-slewing (tracking) time and adding slewing corrections on top of those.

Another issue we identified is the inclinometer sensor providing mirror elevation for gravity compensation distribution. The inclinometer's signal, measuring a body's fall vector due to acceleration in the gravity field, is naturally affected by the body's own acceleration.[14] As this problem was discovered late in the testing, we plan to solve it when the mirror is on the telescope.

4.2 Soak Tests and ICS Performance

The performance of the inertia compensation system directly affects the measured forces on the hardpoints. Since the ICS controls the FAs to hold all the static and inertia forces during a slew, the hardpoints should not receive any load. To be even more specific, it is critical that the ICS maintains the forces on the hardpoints within their breakaway limits. When running the survey, the forces measured on the HPs shall consistently remain within the long-term safe operational limits (15% of the breakaway limits).

As mentioned before, we started these tests by limiting the maximum velocity, acceleration, and jerk with a fraction of 10% the values in table 1 and slowly increased these limits up to 100% of these values. See Figure 7 for an example of a slew performed at maximum velocity, acceleration, and jerk. The figure shows that, during the whole slew, the measured forces on the hardpoints stay inside the region defined by the red continuous lines at the top and at the bottom of the plot representing the nominal breakaway limit of 3000 N defined in the sub-section 3.2. However, it also shows that these forces crossed the dashed red line at 30% of the nominal breakaway limit. Again, the 30% breakaway limit represents the glass stress or fatigue limit. Keeping the measured forces in the hardpoints below this fatigue limit minimizes long-term stress and fatigue effects in the mirror.

Figure 8 shows another 3.5 deg slew from a soak test running at a maximum velocity, acceleration, and jerk limited to 40% of the values in table 1. It shows that the measured forces in this configuration are much smaller. In fact, they are within the operational limit defined in Section 2 above and represented as a red-dotted line.

Figures 9 and 10 show histograms containing the maximum and minimum forces measured on the hardpoints on all the slews performed during a single night. In both figures, the blue bars represent gateway tests, and the orange bars represent soak tests over two different nights. Both plots include the same representation of the breakaway limits (continuous red line), fatigue limits (dashed red line), and operational limits (dotted red line). The BLOCK code is an internal index used to identify our tests. BLOCK-178, in blue, represents the gateway tests. BLOCK-146, in orange, represents soak tests.

The slews in the gateway tests on Figure 9 were executed with a maximum velocity, acceleration, and jerk of 40% and 70% of the values represented in table 1. This explains the large spread in the number of slews

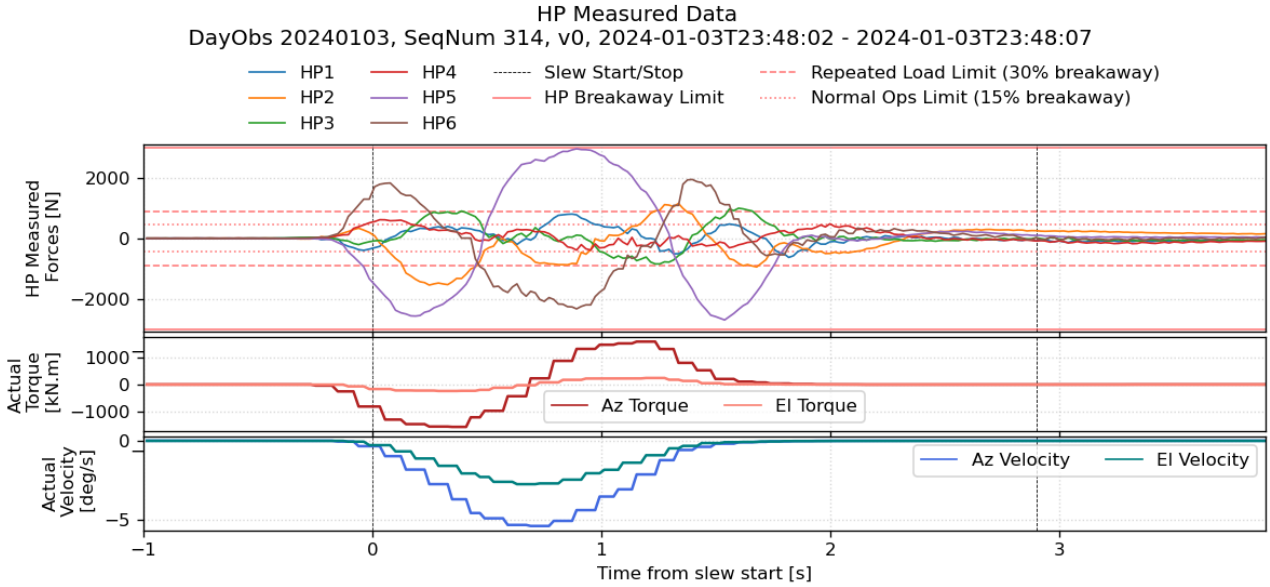

Figure 7. ICS performance when performing a 3.5 deg slew at 100% velocity, acceleration, and jerk. The top y-axes show the measured hardpoint forces. The middle and bottom y-axes show the torques and velocities for Azimuth in Elevation over the same time window. Since the measured forces are trespassing the fatigue limit, running the survey in this configuration can cause damage to the mirror.

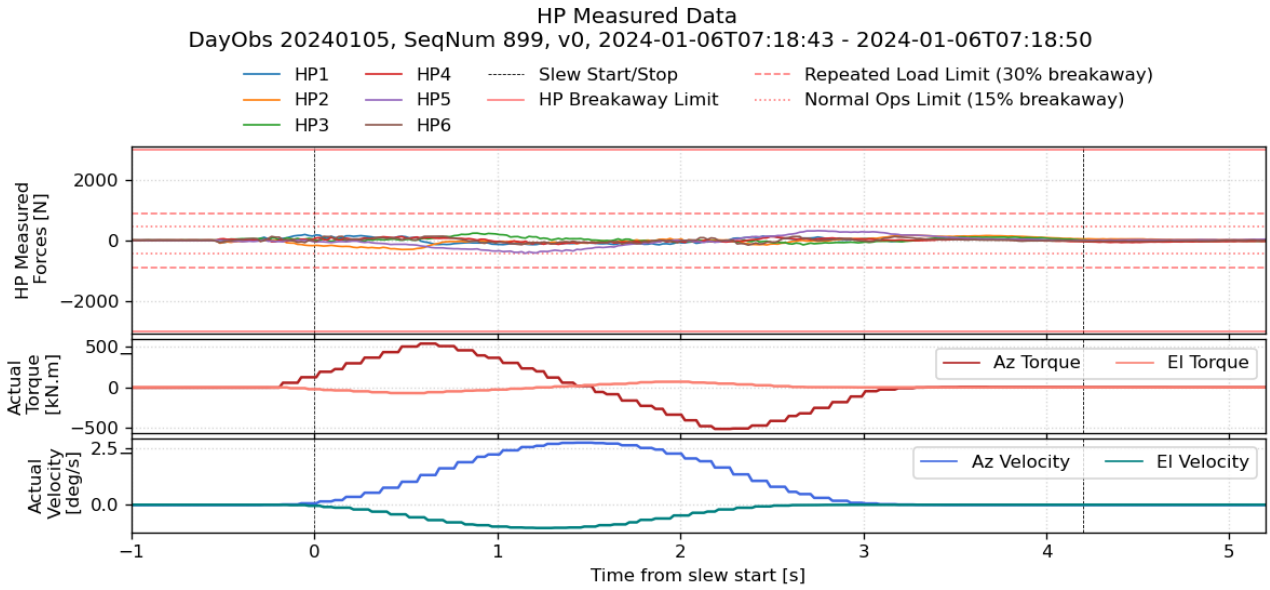

Figure 8. ICS performance when performing a 3.5 deg slew at 40% velocity, acceleration, and jerk. For this configuration, the measured forces are within the operational limits.

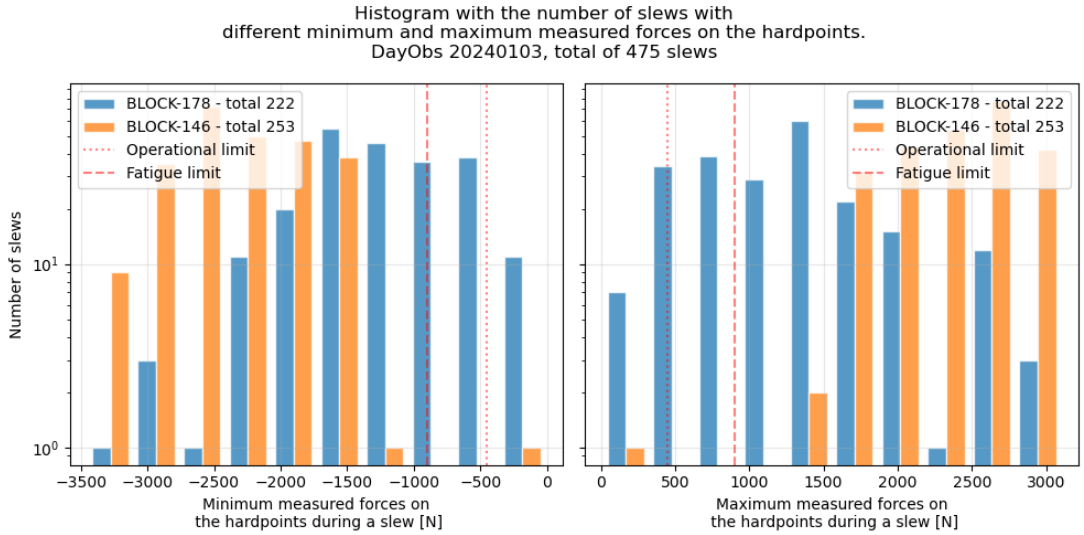

Figure 9. Histogram showing the count of slews performed at 100% velocity, acceleration, and jerk that reached a certain minimum and maximum values during a slew.

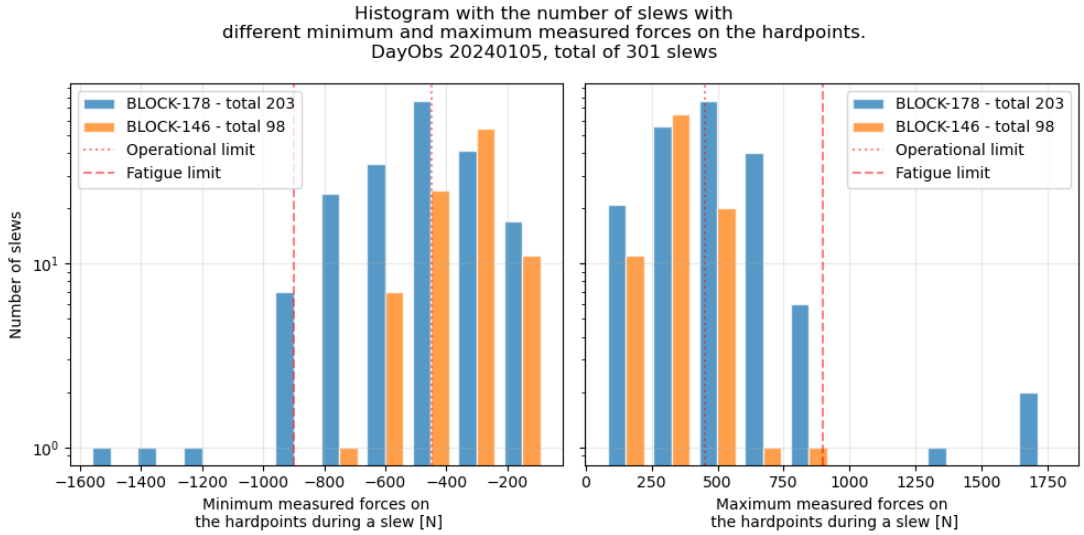

Figure 10. Histogram showing the count of slews performed at 40% velocity, acceleration, and jerk that reached a certain minimum and maximum values during a slew.

of different maximum and minimum measured forces. The figure shows how both positive and negative fatigue limits are trespassed by an important number of slews when running this test. The slews associated with the soak test in this same figure were performed with maximum velocity, acceleration, and jerk. We can see here that almost every slew performed in this configuration trespasses both negative and positive fatigue limits, which would be an important danger to the mirror in the long term.

Figure 10 shows the same two tests, but the maximum velocity, acceleration, and jerk are set to 40% of the value in table 1 in both cases. This configuration helps to disentangle the data presented in the previous plot, and we can see that most of the slews performed during gateway tests are near or within the fatigue limits. In addition to that, almost every slew obtained during soak tests remains inside the fatigue limits, and the majority are near or within the operational limits.

5. CONCLUSION

Our static tests using the M1M3 steel surrogate showed that the M1M3 Cell provides a safe system capable of handling gravitational and residual forces applied to the mirror. This ensures glass safety upon installation on the cell. We ensured that the system was capable of properly handling the mirror weight at different elevation angles and that we could move the telescope at low speeds.

The transition from static to dynamic testing allowed us to explore new territory in terms of testing, validating, and improving the inertia compensation system to the point where we could operate the telescope at up to 40% of its maximum capacity under controlled conditions. Integrating accelerometers and the FBS to counteract acceleration and velocity forces was crucial to reaching such a limit. The maximum slew performance allowed by the ICS is still below the minimum required performance of 70% of the maximum velocity, acceleration, and jerk, which is critical for successfully completing the Legacy Survey of Space and Time (LSST). However, we have proven ourselves capable of operating the telescope while keeping the mirror safe even during a development phase until we reach the maximum slew settings allowed by the telescope.

As we prepare for the next significant phase of installing the M1M3 glass on the M1M3 cell and on the TMA, we are exploring several enhancements to the M1M3 support system to optimize the reaction to inertial forces. The primary proposed change is to increase the pressure in the M1M3 from 120 psi to approximately 130 psi. This adjustment is expected to significantly enhance the dynamics of the force actuators (FAs), enabling them to build up force more rapidly and effectively counteract inertia. The need for this adjustment has been identified through measurements indicating that the current time for force buildup by the actuators is insufficient compared to the acceleration forces applied during telescope slews.

Additional improvements include implementing direct feedback from the newly operational gyroscope to refine velocity force adjustments, which could potentially reduce forces by as much as 500 N per axis. This would complement the current force-balancing strategy, enhancing overall system performance. Regular maintenance to improve leak sealing within the force actuators is also planned. This maintenance is crucial as some FAs have been observed to lose air, especially when booster valves are activated, impacting their dynamic response. Lastly, discussions about preloading the system for anticipated forces were considered but ultimately rejected due to the unpredictability of actual telescope movements and the potential risks of premature system response.

With these improvements in place, we will conduct a comprehensive reiteration of all previously described tests. The process will commence with a re-verification of safety interlocks and system functionalities, following the same initial procedures used with the surrogate. We will then repeat both quasi-static and dynamic tests using the actual glass, starting with slews at low velocities, accelerations, and jerks. As the glass safety is confirmed over these initial tests, we will incrementally increase the operational parameters, mirroring the approach successfully applied with the surrogate. Successfully reaching slews at the telescope's maximum performance levels while keeping the measured forces in the hardpoints within safe operational limits is essential both to guarantee the long-term safety of the glass and ensure the Vera Rubin Observatory is prepared to successfully undertake the Legacy Survey of Space and Time.

ACKNOWLEDGMENTS

This material is based upon work supported in part by the National Science Foundation through Cooperative Agreement AST-1258333 and Cooperative Support Agreement AST-1202910 managed by the Association of Universities for Research in Astronomy (AURA) and the Department of Energy under Contract No. DE-AC02-76SF00515 with the SLAC National Accelerator Laboratory managed by Stanford University. Additional Rubin Observatory funding comes from private donations, grants to universities, and in-kind support from LSSTC Institutional Members.

REFERENCES

[1] Ivezić, Ž., Kahn, S. M., Tyson, J. A., Abel, B., Acosta, E., Allsman, R., Alonso, D., AlSayyad, Y., Anderson, S. F., Andrew, J., et al., "LSST: From Science Drivers to Reference Design and Anticipated Data Products," *Astrophysical Journal* **873**, 111 (Mar. 2019). DOI: https://doi.org/10.3847/1538-4357/ab042c.

[2] Neill, D. R., Hileman, E., Sebag, J., Gressler, W., Wiecha, O., Warner, M., Andrew, J., and Schoening, B., "Baseline design of the LSST telescope mount assembly," in [*Ground-based and Airborne Telescopes V*], Stepp, L. M., Gilmozzi, R., and Hall, H. J., eds., *Society of Photo-Optical Instrumentation Engineers (SPIE) Conference Series* **9145**, 914518 (July 2014). DOI: https://doi.org/10.1117/12.2056432.

[3] Sebag, J., Andrew, J., Angeli, G., Araujo, C., Barr, J., Callahan, S., Cho, M., Claver, C., Daruich, F., Gressler, W., et al., "LSST telescope modeling overview," in [*Modeling, Systems Engineering, and Project Management for Astronomy VI*], Angeli, G. Z. and Dierickx, P., eds., *Society of Photo-Optical Instrumentation Engineers (SPIE) Conference Series* **9911**, 99112E (Aug. 2016). DOI: https://doi.org/10.1117/12.2233178.

[4] Felipe Daruich, Christian Aguilar, Claudio Araya, Karla Aubel, Erich Bugeno, et al., "Rubin Observatory primary and tertiary (M1M3) mirror cell assembly final integration and commissioning," in [*Ground-based and Airborne Telescopes X*], Marshall, H. K., Spyromilio, J., and Usuda, T., eds., *Society of Photo-Optical Instrumentation Engineers (SPIE) Conference Series* **13094**, 13094–222 in press (2024). https://dx.doi.org/doi#here.

[5] Neill, D. R., Muller, G., Hileman, E., DeVries, J., Araujo, C., Gressler, W. J., Lotz, P. J., Mills, D., Sebag, J., Thomas, S., Warner, M., and Wiecha, O., "Final design of the LSST primary/tertiary mirror cell assembly," in [*Ground-based and Airborne Telescopes VI*], Hall, H. J., Gilmozzi, R., and Marshall, H. K., eds., *Society of Photo-Optical Instrumentation Engineers (SPIE) Conference Series* **9906**, 99060Q (July 2016). DOI: https://doi.org/10.1117/12.2234016.

[6] Booth, M. T., Clements, A., and Johnson, B., "LSST hardpoints final design, fabrication, and test," in [*Ground-based and Airborne Telescopes VII*], Marshall, H. K. and Spyromilio, J., eds., *Society of Photo-Optical Instrumentation Engineers (SPIE) Conference Series* **10700**, 107003S (July 2018). DOI: https://doi.org/10.1117/12.2312671.

[7] Ashby, D. S., Kern, J., Hill, J. M., Davison, W. B., Cuerden, B., Brynnel, J. G., Biddick, C., and Duffek, K., "The Large Binocular Telescope primary mirror support control system description and current performance results," in [*Advanced Optical and Mechanical Technologies in Telescopes and Instrumentation*], Atad-Ettedgui, E. and Lemke, D., eds., *Society of Photo-Optical Instrumentation Engineers (SPIE) Conference Series* **7018**, 70184C (July 2008). DOI: https://doi.org/10.1117/12.790072.

[8] Booth, M. T., Clements, A., and Johnson, B., "LSST hardpoints final design, fabrication, and test," in [*Ground-based and Airborne Telescopes VII*], Marshall, H. K. and Spyromilio, J., eds., *Society of Photo-Optical Instrumentation Engineers (SPIE) Conference Series* **10700**, 107003S (July 2018). DOI: https://doi.org/10.1117/12.2312671.

[9] Muller, G. P., Hileman, E. A., Daruich, F., Warner, M., Wiecha, O. M., Araujo, C., Mills, N. G., Johnson, B. E., Stover, E., Booth, M. T., et al., "LSST M1M3 figure actuator final design, fabrication, and test," in [*Ground-based and Airborne Telescopes VII*], Marshall, H. K. and Spyromilio, J., eds., *Society of Photo-Optical Instrumentation Engineers (SPIE) Conference Series* **10700**, 107003V (July 2018). DOI: https://doi.org/10.1117/12.2313598.

[10] Neill, D., Angeli, G., Claver, C., Hileman, E., DeVries, J., Sebag, J., and Xin, B., "Overview of the LSST active optics system," in [*Modeling, Systems Engineering, and Project Management for Astronomy VI*], Angeli, G. Z. and Dierickx, P., eds., *Society of Photo-Optical Instrumentation Engineers (SPIE) Conference Series* **9150**, 91500G (Aug. 2014). DOI: https://doi.org/10.1117/12.2056553.

[11] Daruich, F., Neill, D., Warner, M., Hileman, E., Cho, M., Dribusch, C., Araujo, C., Booth, M., Contaxis, C., Harris, R., et al., "LSST M1M3 active mirror support system optimized to accommodate rapid telescope motions," in [*Ground-based and Airborne Telescopes VII*], Marshall, H. K. and Spyromilio, J., eds., *Society of Photo-Optical Instrumentation Engineers (SPIE) Conference Series* **10700**, 107003G (July 2018). DOI: https://doi.org/10.1117/12.2313724.

[12] Megias Homar, G., Meyers, J. M., Thomas, S., Kahn, S. M., Connolly, A., Crenshaw, J. F., Kalmbach, B., Suberlak, C., Polen, R., Tsai, T.-W., and Ribeiro, T., "Advancing the Vera C. Rubin active optics control system," in [*Ground-based and Airborne Telescopes X*], Marshall, H. K., Spyromilio, J., and Usuda, T., eds., *Society of Photo-Optical Instrumentation Engineers (SPIE) Conference Series* **13094**, 13094–205 in press (2024). https://dx.doi.org/doi#here.

[13] Brian Stalder, Freddy Muñoz Arancibia, Jeffrey Barr, Andy W. Clements, Felipe Daruich, et al., "Rubin Observatory Simonyi Survey Telescope integrated mount performance," in [*Ground-based and Airborne Telescopes X*], Marshall, H. K., Spyromilio, J., and Usuda, T., eds., *Society of Photo-Optical Instrumentation Engineers (SPIE) Conference Series* **13094**, 13094–8 in press (2024). https://dx.doi.org/doi#here.

[14] Mitikiri, Y. and Mohseni, K., "Acceleration compensation for gravity sense using an accelerometer in an aerodynamically stable uav," in [*2019 IEEE 58th Conference on Decision and Control (CDC)*], 1177–1182, IEEE (2019).